HHS Public Access

Author manuscript

Biochim Biophys Acta. Author manuscript; available in PMC 2017 June 01.

Published in final edited form as:

Biochim Biophys Acta. 2016 June ; 1858(6): 1362–1372. doi:10.1016/j.bbamem.2016.03.007.

The ionization properties of cardiolipin and its variants in model bilayers

Murugappan Sathappa and **Nathan N. Alder***

Department of Molecular and Cell Biology, University of Connecticut, Storrs, CT 06269, United States

Abstract

The anionic phospholipid cardiolipin has an unusual dimeric structure with a two-phosphate headgroup and four acyl chains. Cardiolipin is present in energy-transducing membranes that maintain electrochemical gradients, including most bacterial plasma membranes and the mitochondrial inner membrane, where it mediates respiratory complex assembly and activation, among many other roles. Dysfunctional biogenesis of cardiolipin is implicated in the pathogenesis of several diseases including Barth syndrome. Because cardiolipin is a dominant anionic lipid in energy-conserving membranes, its headgroup is a major contributor to surface charge density and the bilayer electrostatic profile. However, the proton dissociation behavior of its headgroup remains controversial. In one model, the pK_a values of the phosphates differ by several units and the headgroup exists as a monoanion at physiological pH. In another model, both phosphates ionize as strong acids with low pK_a values and the headgroup exists in dianionic form at physiological pH. Using independent electrokinetic and spectroscopic approaches, coupled with analysis using Gouy–Chapman–Stern formalism, we have analyzed the ionization properties of cardiolipin within biologically relevant lipid bilayer model systems. We show that both phosphates of the cardiolipin headgroup show strong ionization behavior with low pK_a values. Moreover, cardiolipin variants lacking structural features proposed to be required to maintain disparate pK_a values – namely the secondary hydroxyl on the central glycerol or a full complement of four acyl chains – were shown to have ionization behavior identical to intact cardiolipin. Hence, these results indicate that within the physiological pH range, the cardiolipin headgroup is fully ionized as a dianion. We discuss the implications of these results with respect to the role of cardiolipin in defining membrane surface potential, activating respiratory complexes, and modulating membrane curvature.

Keywords

Cardiolipin; Mitochondria; Lipid ionization; Barth syndrome

*Corresponding author at: Department of Molecular and Cell Biology, University of Connecticut, 91 N. Eagleville Rd., Storrs, CT 06269-3125, United States. ; Email: nathan.alder@uconn.edu (N.N. Alder)

Transparency document

The transparency document associated with this article can be found in the online version.

1. Introduction

The anionic phospholipid cardiolipin (CL; 1,3-*bis*(*sn*-3′-phosphatidyl)-*sn*-glycerol) is found in energy-transducing membranes that couple electrochemical potentials with endergonic processes such as ATP synthesis and metabolite transport. Such membranes include the plasma membrane of most bacteria and the mitochondrial inner membrane. Among phospholipids, CL has an unusual dimer-like structure with two 1,2-diacyl phosphatidate moieties esterified to the 1- and 3-hydroxyls of a central glycerol bridge; hence, each CL molecule contains four acyl chains and two phosphate groups (Fig. 1). CL is essential for the activation of complexes involved in oxidative phosphorylation (OXPHOS) and their assembly into higher-order supercomplexes [1–4]. Within mitochondria this lipid is a central player in many processes including apoptosis, mitophagy, protein biogenesis, establishment of cristae morphology, and organelle dynamics [5–8]. In its myriad roles, CL specifically interacts with a range of integral and peripheral membrane proteins, and recent structural and computational studies have made significant progress in elucidating the nature of the protein binding sites that interact with its headgroup and acyl chain regions [9]. Altered CL metabolism has been implicated in the pathogenesis of many diseases, including diabetes, cardiovascular disease, neurodegenerative disease, and the multisystem disease Barth syndrome (see below) [10–13].

The dimeric structure of CL imparts specific physical and chemical properties that are central to its function [14]. Because two phosphatidates are bound to a single central glycerol headgroup, CL assumes a more conical shape in which the cross sectional area of the polar headgroup is smaller than that occupied by the fatty acid chains. This molecular geometry increases lateral pressure within the acyl chain region [15] and promotes the transition from bilayer to non-bilayer phases with strong negative curvature, particularly when the headgroup surface charges are screened by protonation [16,17] or high ionic strength [18], as well as upon binding to mono- and divalent metal cations [19,20], polybasic proteins [21] or positively charged lipids [22,23]. Information on the orientation and dynamics of CL within the bilayer comes from ^{2}H-NMR spectroscopic studies [24]. This work indicated that the headgroup glycerol of CL is parallel to the bilayer surface, that the two 1,2-acylated backbone glycerol groups are, as for other phospholipids, parallel to the bilayer normal, and that the CL headgroup is motionally constrained compared with other lipids. The latter point suggests that within a lipid bilayer, inter- and intramolecular hydrogen bonding interactions of the CL headgroup are hindered, except to solvent and dissolved molecules in the interfacial region.

The acyl chain profile of CL is atypical among phospholipids. Despite the diversity of fatty acid combinations theoretically possible for this tetraacyl lipid, only a few types of unsaturated acyl groups are actually represented for CL within a given organism or tissue type [25]. In eukaryotes, this structural uniformity results from acyl chain remodeling processes (cycles of deacylation and reacylation) that occur following the *de novo* synthesis of nascent CL at the mitochondrial inner membrane [26–30]. In yeast, newly synthesized CL, which primarily contains saturated fatty acids, is deacylated by a CL-specific phospholipase to produce monolyso-CL (MLCL) [31]. Tafazzin, a CoA-independent transacylase, then transfers an unsaturated fatty acid from a donor lipid to MLCL [32].

Because CL biogenesis is an evolutionarily conserved process, the remodeling steps are similar in mammals, with two main exceptions: (i) a different phospholipase has been implicated in CL remodeling [33], and additional deacylases may be involved, and (ii) acyltranferases in the ER and mitochondrial matrix, in addition to tafazzin, have been implicated in the reacylation of MLCL [34–36]. Moreover, because tafazzin can catalyze both the removal and reattachment of acyl chains, this enzyme alone can catalyze CL remodeling by a single-step transacylation reaction. The importance of tafazzin-mediated CL remodeling is underscored by Barth syndrome, which results from nonsense or missense mutations in the X-linked *TAZ* gene and presents with cardiac and skeletal myopathies, cyclic neutropenia, and growth disturbance, and can be fatal in young males [37]. With reduced amounts of CL, altered acyl chain profiles and an accumulation of MLCL, Barth syndrome patients have abnormal mitochondrial ultrastructure and destabilized respiratory supercomplexes [38–42].

As a predominant anionic lipid within energy-transducing membranes, CL largely defines the surface charge properties of these bilayers. Indeed, most biomembranes carry a net negative surface charge at physiological pH, owing in part to the abundance of anionic lipids [43]. CL is the major anionic phospholipid of the mitochondrial inner membrane, typically amounting to 10–20 mol% of the total lipids [44]. As such, the formal charge of the two-phosphate CL headgroup largely defines the electrostatic properties in the interfacial region, which in turn regulates processes including polymorphic phase behavior, establishment of membrane curvature, charge–charge interactions with peripheral and integral membrane proteins, and headgroup coordination of ions.

Yet despite years of research, the ionization behavior of the CL headgroup remains controversial. The phosphodiester groups of most typical phospholipids behave as strong acids, with measured pK_a values ranging between 1 and 3, consistent with the first pK_a of phosphoric acid (pK_a 2.15) [45,46]. Therefore, in the absence of CL-specific intra- or inter-molecular interactions that would significantly influence its ionization properties, it would be expected that the two phosphates of CL would each have similarly low pK_a values. As a corollary, CL would exist as a dianion at physiological pH (Fig. 1A). Indeed, early work based on micro-electrophoresis [47], acid hydrolysis [48] and pH-induced phase transitions from lamellar (Lα) to inverted hexagonal (H_{II}) structures [16] supported the notion that the two CL phosphates are strong acids, being ionized at low bulk pH.

However, based on pH titration experiments, Haines and colleagues concluded that the two phosphate diesters of CL have quite disparate pK_a values: one that is low (pK_1 ~ 2–4) and the other that extends beyond the neutral pH range (pK_2 > 8.5) [49]. The proposed model to account for the unusually high pK_2 was a resonance-stabilized acid-anion based on a bicyclic head group structure in which the protonated state of one phosphate oxygen atom is stabilized by hydrogen bond interactions with the secondary hydroxyl of the central glycerol [49,50] (Fig. 1B). Established as the paradigm for CL ionization for many years, this model is attractive for several reasons. Mechanistically, if the CL head group traps a proton in the interfacial region, it can buffer protons, acting as a proton reservoir for proton-pumping respiratory enzymes with a low energetic barrier to protonation or de-protonation of the lipid [51,52]. Moreover, it was proposed that equal lengths of the four acyl chains could stabilize

the bicyclic structure; therefore, this model could explain the requirement for CL remodeling and chain symmetry [53]. By coupling the balance of acyl chain length to head group ionization, this model could provide one mechanistic underpinning for Barth syndrome. Specifically, a disruption to acyl chain symmetry or, more drastically the loss of an acyl chain (as in MLCL), might bring the hydrocarbon chains out of register, thereby destabilizing the head group structure and affecting the ionized state of the phosphates. More recently, support for disparate pK_a values of CL phosphates has come on many fronts. For instance, surface force measurements suggest that at neutral pH, the fraction of ionized CL phosphates decreases with increasing molar concentrations of CL [54], Fourier transform infrared (FTIR) spectroscopy measurements support two widely separated pK_a values [55], and liquid crystal-detected ordering transitions indicate monoanionic CL species at intermediate pH values [56]. Moreover, molecular dynamics simulations support the feasibility of intramolecular hydrogen bonding within the CL headgroup [57–60].

By contrast, other groups have provided evidence that CL phosphates both behave as strong acids with low pK_a values. For example, studies monitoring phase transitions of CL-containing bilayers with different cationic lipids strongly suggest that CL is fully ionized near neutral pH [22,23]. A more recent study, based on pH titration and calorimetric measurements with aqueous dispersions of synthetic CL, provided evidence that the CL headgroup behaves as a strong dibasic acid, with both phosphate pK_a values between 2 and 3 [61]. Moreover, a recent FTIR analysis of CL-containing liposomes supported the view that the headgroup phosphates were fully ionized at neutral pH [62]. These experimental results are clearly at odds with the dominant model that proposed very different ionization behavior for the two CL phosphates. Moreover, from a theoretical standpoint, the intramolecular hydrogen bonding network required to stabilize the disparate pK_a values does not appear to be an energetically favorable conformation. As described above, conformational constraints of the glycerol headgroup would render such hydrogen bonding unlikely [14,24]. Also, as noted [61], the difference in pK_2 between CL and dCL reported by Haines and colleagues strongly exceeds that caused by introducing hydroxyl groups into organic acids of similar size, and would require a very large stabilization energy of the intramolecular hydrogen bond (upwards of 35 kJ mol^{-1}).

The ionization behavior of the CL headgroup therefore remains controversial. This is a critical issue to resolve because CL ionization is fundamental to: (i) the surface charge density (and surface electrostatic potential) of CL-rich energy-conserving membranes; (ii) pH-dependent conformations and polymorphic behavior of CL; and (iii) the mechanism by which CL promotes the activity of respiratory enzymes. To address the pH-dependent ionization of CL, we have performed independent electrokinetic and spectroscopic evaluations of CL and CL variants within physiologically relevant bilayer mimetics of the mitochondrial inner membrane. We conclude that the phosphate groups of CL both have low intrinsic pK_a values, and that neither the loss of the hydroxyl group of the central glycerol nor the loss of an acyl chain affects its headgroup ionization.

2. Materials and methods

2.1. Preparation of unilamellar lipid vesicles

Synthetic phospholipids were purchased as chloroform stocks from Avanti Polar Lipids, including: 1-palmitoyl-2-oleoyl-*sn*-glycero-3-phosphocholine (POPC), 1-palmitoyl-2-oleoyl-*sn*-glycero-3-phosphoethanolamine (POPE), 1-palmitoyl-2-oleoyl-*sn*-glycero-3-phosphoglycerol (POPG), 1-palmitoyl-2-oleoyl-*sn*-glycero-3-phosphoserine (POPS), 1-palmitoyl-2-oleoyl-*sn*-glycero-3-phosphate (POPA), and variants of cardiolipin with 18:1 acyl chains, including 1′,3′-bis[1,2-dioleoyl-*sn*-glycerol-3-phospho-]-*sn*-glycerol (TOCL), 2′-deoxycardiolipin (dCL), and monolyso-cardiolipin (MLCL). All stocks were stored at −20 °C until use. Liposomes of specific lipid composition were prepared by first mixing stocks at the appropriate molar ratio and drying under a nitrogen stream for 20 min in a glass test tube, followed by overnight evaporation in a vacuum desiccator to remove all organic solvent. Lipid films were hydrated in application-specific aqueous buffer (described below) for 30 min with stirring to produce a solution of 3 to 5 mg lipids ml^{-1}. The resulting multilamellar vesicles were then passed 17 or 19 times through a Mini-Extruder (Avanti) with polycarbonate filter to yield large unilamellar vesicles (LUVs) of the desired diameter. LUVs for zeta potential measurements contained a background of 80 mol% zwitterioic host lipids (POPC and POPE in equal molar proportions) and 20 mol% anionic test lipid (CL, dCL, MLCL, POPG, POPS or POPA). Depending on the target pH, these LUVs were hydrated in 10 mM NaCl and either 10 mM phosphate–citrate buffer (pH range 2.0 to 8.0) or 10 mM AMPD (pH range 8.0 to 9.7) and extruded through 0.4 μm filters. LUVs for fluorescence measurements were composed of POPC host lipids, containing either 30, 50 or 70 mol% POPG or 50 mol% anionic test lipids (CL, dCL or MLCL). These LUVs were hydrated in 25 mM HEPES-KOH, pH 7.5, and extruded using 0.1 μm filters.

2.2. Zeta potential measurements and data analysis

The zeta potential (ζ) of unilamellar vesicles, representing the electrostatic potential at the hydrodynamic plane of shear, was measured using a ZetaPlus Zeta Potential Analyzer (Brookhaven Instruments Corp., Holtsville, NY). LUVs (1 mg lipid ml^{-1}) were added to buffer systems of different pH (10 mM phosphate–citrate for pH 2–8 and 10 mM AMPD for pH 8–10) that included 10 mM NaCl. Values for ζ were based on measurements of vesicle electrophoretic mobility (μ) per the Helmholtz-Smoluchowski equation:

$$\zeta = \frac{\mu\eta}{\varepsilon_r \varepsilon_0} \quad (1)$$

where ε_r is the dielectric constant of the aqueous phase, ε_0 is the permittivity of free space, and η is the viscosity of the solution [63]. At least three independent samples were measured for each lipid composition type. The analysis and modeling of zeta potential measurements were performed as follows:

2.2.1. Gouy–Chapman–Stern formalism—The electrostatic profile of the diffuse double layer perpendicular to the bilayer plane in the aqueous phase is modeled from the

Gouy–Chapman equation, which is based on the non-linear Poisson–Boltzmann relationship [64,65]

$$\frac{d^2\psi_x}{dx^2} = -\frac{1}{\varepsilon_r \varepsilon_0} \sum_i Z_i F C_i \exp\left(\frac{-Z_i F \psi_x}{RT}\right) \quad (2)$$

where ψ_x is the electrostatic potential at a distance x from the membrane relative to the potential of the bulk phase ($\psi_\infty = 0$), C_i is the concentration of ions of valence Z_i, F is the Faraday constant, and R is the universal gas constant. Given the appropriate boundary conditions and noting that the membrane surface charge is balanced by charges in the diffuse layer, the integrated form of the Gouy–Chapman equation yields the relationship between the surface charge density (σ) and the surface potential (ψ_0):

$$\sigma = \frac{\psi_0}{|\psi_0|}\left[2\varepsilon_r \varepsilon_0 RT \sum_i C_{i\infty}\left(\exp\left(\frac{-Z_i F \psi_0}{RT}\right) - 1\right)\right]^{1/2}. \quad (3)$$

The distribution of ions in the direction normal to the membrane surface is determined by Boltzmann statistics:

$$C_{ix} = C_{i\infty} \exp\left(\frac{-Z_i F \psi_x}{RT}\right) \quad (4)$$

where C_{ix} and $C_{i\infty}$ are, respectively, the concentrations of species i of valence Z_i at a distance x from the bilayer and in the bulk solution.

The membrane surface charge density was evaluated using a Langmuir adsorption isotherm [66] to account for ionic interactions and charges on titratable head group sites. Each charged group per lipid bears an intrinsic surface charge density $\sigma^{max} = \pm e/A$, where e is an electronic charge and A is the cross-sectional area of the lipid (A = 70 Å^2 for all lipids other than CL, for which a value of 140 Å^2 is used [60]). Thus, the molar fraction of lipid j (χ_j) in a composite bilayer determines the maximal surface charge imparted by that particular species and $\sigma^{max_j} = (\pm e/A_j)\chi_j$. Under a given set of conditions, the actual surface charge density (σ^{net}) is modulated by two factors. First, counter-ions from solution electrolytes (cations, C^+ or anions, A^-) will bind to sites of fixed charge (ionized lipid headgroups) at the bilayer surface with association constants K_C and K_A, respectively. Second, the charge of each titratable headgroup function (phosphate or amine) with a given intrinsic pK_a value will be determined by the pH at the bilayer surface. The effective charge density therefore takes the form:

$$\sigma = \sum \frac{\sigma^{\max A}}{1 + \left(\frac{[H^+]_{x=0}}{K_a} + K_C [C^+]_{x=0}\right)} + \sum \frac{\sigma^{\max B}}{1 + \left(\frac{K_a}{[H^+]_{x=0}} + K_A [A^-]_{x=0}\right)} \quad (5)$$

where *A* denotes acidic sites (those whose protonation results in deionization) and *B* denotes basic sites (those whose protonation results in ionization). From Eq. 4, the concentrations of protons, monovalent cations, and monovalent anions at the surface (x = 0) are as follows:

$$[\mathrm{H}^+]_{x=0}=[\mathrm{H}^+]_\infty \exp(-38.94\psi_0), [\mathrm{C}^+]_{x=0} =[\mathrm{C}^+]_\infty \exp(-38.94\psi_0) \text{ and } [\mathrm{A}^-]_{x=0}=[\mathrm{A}^-]_\infty \exp(38.94\psi_0)$$

where the subscript ∞ denotes bulk concentrations and T = 298 K. Eqs. 3–5 were evaluated simultaneously (Wolfram *Mathematica* 10) to determine ψ_0, σ, and K_a values as described in the text. Further explanation and graphical analyses of this approach are given in Supplementary Text, Sections A1 and A2 (Figs. S1 and S2).

2.2.2. Calculation of ψ_0—Evaluation of ψ_0 was based on zeta potential measurements ($\psi_\zeta = \psi_x$, where x is the distance of the hydrodynamic plane of shear from the membrane surface) using the following relationship to describe the distance-dependent decay of the potential from the membrane surface

$$\kappa x=\ln\left\{\frac{[\exp(ZF\psi_x/2RT)+1][\exp(ZF\psi_0/2RT)-1]}{[\exp(ZF\psi_x/2RT)-1][\exp(ZF\psi_0/2RT)+1]}\right\} \quad (6)$$

where κ, the Debye constant, is:

$$\kappa=\left(\frac{2Z^2F^2C_{i\infty}}{\varepsilon_r\varepsilon_0RT}\right)^{1/2} \quad (7)$$

Distance-dependent electrostatic profiles calculated as above are illustrated and explained in Supplementary Text, Section A3 (Fig. S3). To determine the ionization properties of the lipids used in our experiments, measured ψ_ζ values were used to calculate the corresponding ψ_0 values, which were then used in Eqs. 3–5 above. The electrostatic shear plane was assumed to be at x = 2 Å [66]. Additional explanation of the effects of electrolyte concentration and binding constants on ψ_0 and σ by this model is provided in Supplementary Text, Section A3 (Fig. S4).

2.3. Analytical fluorescence measurements of surface potential

9-Aminoacridine (9-AA) was used as a fluorescent probe to evaluate the surface charge densities of model membranes based on its accumulation and self-quenching in the diffuse layer [67–70]. Steady-state measurements of 9-AA fluorescence (λ_{ex} = 400 nm; λ_{em} = 455 nm) were performed with a Fluorolog 3–22 spectrofluorometer (HORIBA Jobin-Yvon) equipped with photon-counting electronics, double-grating excitation and emission monochromators and a 450-W xenon lamp. For each time course measurement, a low salt solution with buffer (25 mM HEPES-KOH, pH 7.5) containing 20 μM 9-AA and LUVs (0.1 mg lipid ml^{-1}) containing variable concentrations of anionic lipid was subjected to repeated

additions of the organic cation decamethonium bromide (DM^{2+}) from a concentrated stock solution. For each titration point, the average relative fluorescence intensity (F) was recorded and normalized by the maximal fluorescence (F_{max}), recorded following the addition of 10 mM $MgCl_2$. For each experiment, POPG-containing liposomes were measured in parallel as membranes with a known net charge per unit area in comparison with liposomes containing CL variants (TOCL, dCL or MLCL).

Determination of the σ of CL-containing membranes was predicated on the ψ_0-dependent accumulation of the 9-AA cation at the bilayer interface and on the assumption that for different lipid systems, ψ_0 is equivalent when 9-AA quenching (quantified at F/F_{max}) is identical. Thus, F/F_{max} equivalence points between POPG- and CL-containing samples were identified for each titration, the ψ_0 was calculated for POPG samples at specific points, and based on these ψ_0 values, the σ values of CL-containing membranes were determined by a nonlinear least squares procedure based on the Gouy–Chapman–Stern formalism described above. A graphical explanation of this analysis is provided in Supplementary Text, Section B (Fig. S5).

2.4. Vesicle size determination by dynamic light scattering

The hydrodynamic size distributions of liposomes at various pH values were measured using dynamic light scattering (Zetasizer Nano S90, Malvern Instruments, United Kingdom). Values reported in this study include intensity-weighted average diameter for all size populations (Z-average) and the polydispersity index (PI). The measurements were performed in a buffer solution of 10 mM phosphate citrate (pH 2 to 7) with 10 mM NaCl at 25 °C. Each sample was measured in three successive runs at one minute intervals. The scattering data were analyzed by Zetasizer software.

3. Results

3.1. The relationship between CL ionization behavior and electrostatic properties

The objective of this study was to evaluate the ionization properties of the CL headgroup phosphates within the context of a physiologically relevant lipid bilayer. To this end, we prepared liposomes containing CL (or other anionic lipids for comparison) in a host lipid system of POPC and POPE, designed as a mimetic of the mitochondrial inner membrane. These liposomes were then subjected to independent measurements of the surface potential, ψ_0, as a metric of ionization (and hence surface charge density, σ) under different conditions.

Using Gouy–Chapman–Stern formalism, it is clear that the proposed models of CL ionization (described in the Introduction) would produce profiles of pH-dependent ψ_0 that can be distinguished experimentally. Considering a hypothetical ternary bilayer system of 20 mol% CL in a host of PC/PE lipids, we can compute the pH-dependent ψ_0 and σ, using established values for: (i) the intrinsic pK_a values of the PC and PE titratable headgroup species [45,46], and (ii) association constants of lipid functional groups for solution ions in the diffuse double layer [66]. Fig. 2 shows calculated profiles of ψ_0 and σ as a function of bulk pH for two conditions: case 1 in which both CL phosphates behave as strong acids with low pK_a values, and case 2 in which phosphates have disparate pK_a values. The sizeable

difference in the profiles resulting from these two cases underscores the feasibility of experimentally distinguishing between the two models.

3.2. Zeta potential analysis of cardiolipin ionization within model membranes

As the first approach to evaluating the ionization properties of CL and its variants, we subjected LUVs of defined lipid composition to measurements of ζ potential over a pH range of 2 to 10 within compatible buffer systems. The prepared LUVs consisted of a host background of POPC and POPE with or without 20 mol% anionic phospholipid (TOCL, dCL, MLCL, POPG, POPS, or POPA). Profiles of ζ potential as function of pH were then used to calculate intrinsic pK_a values of the test anionic lipids as follows. First, the relationship between ζ potential and ψ_0 was evaluated based on the Debye constant κ (Eq. 7) and the electrostatic potential profile in the diffuse double layer (Eq. 6) assuming that hydrodynamic shear plane is 2 Å from the bilayer surface. Second, for each pH-specific condition, Gouy–Chapman–Stern analysis was performed by simultaneous evaluation of Eqs. 3–5. The pK_a of the test anionic lipid was evaluated by minimizing the sum of the squares between calculated σ based on electrostatics (Eq. 3) and the protonation/ion binding isotherm (Eq. 5) for all pH conditions.

Fig. 3A shows a composite profile of measured ζ potentials as a function of bulk pH for three types of vesicles: those containing only host lipids, those containing the monoanionic lipid POPG whose ionization properties are well established, and those containing TOCL. As expected, LUVs containing only POPC and POPE (Fig. 3A, diamonds) had negligible ζ potential because within this pH range these zwitterionic lipids do not bear a net charge. Vesicles containing 20 mol% POPG (Fig. 3A, open circles) showed a pH-dependent ζ potential profile that became more negative with increasing pH (as phosphate groups were ionized), and that complete deprotonation of the PG headgroup occurred, as expected, in the low pH region. Evaluation of the intrinsic ionization constant of the POPG phosphate group using the analysis described above returned a value of $pK_a = 0.99$, and the associated curve for this fit is shown by the dashed line. This pK_a value is in excellent agreement with reported values [46], underscoring the accuracy or our analysis and confirming that POPG-containing samples provide good comparators for testing CL-containing samples in parallel. Indeed, the pH-dependent ζ potential profile of vesicles containing 20 mol% TOCL (Fig. 3A, closed circles) indicated that complete ionization of the CL headgroup also occurred within the low pH region. To quantify the ionization properties of the TOCL phosphates based on these data, we assumed that $pK_1 = 1.0$ and computed the value for the second phosphate by the above analysis, which revealed $pK_2 = 1.59$. The curve fit based on these pK_a values is shown by the solid line. Hence, when the pH is above these pK_a values, the CL headgroup would be a dianion, in comparison with the monoanionic PG headgroup.

The difference in ionization properties between the POPG and TOCL phosphates is also demonstrated by comparing the ζ potentials within the pH 6–8 region wherein the phosphates are completely ionized. Within this range, the average ζ potential value for vesicles containing 20 mol% POPG is −48.3 mV (±0.35 SD), compared with that of vesicles with 20 mol% TOCL, which is −58.1 mV (±0.67 SD) (Fig. 3A). To be sure, a lower ζ potential for TOCL-containing vesicles suggests a greater surface charge density (i.e., that

CL headgroups are dianionic, compared with the monoanionic PG headgroups). However, such a comparison must also take into account the cross-sectional area of each lipid (Eq. S5). Because TOCL occupies a greater area than POPG (A = 140 Å^2 vs. 70 Å^2 in our model), an equivalent formal charge per lipid would translate into a higher (less negative) surface charge (and therefore, less negative ψ_0) for TOCL than for POPG. Hence, if TOCL existed as a monoanionc species in this pH range, it would have a less negative ψ_0 than POPG; the fact that the ψ_0 for TOCL-containing vesicles is *lower* than that of POPG-containing ones further confirms that both phosphates of the CL headgroup are ionized. This point is also shown in Fig. 3B, where the measured ζ potential and fit for TOCL-containing vesicles (closed circles, solid line) is shown with the ζ potential profile calculated from our model if TOCL had two disparate pK_a values (pK_1 = 1.0; pK_2 = 8.5). The difference in these two curves further confirms that the phosphates of TOCL behave as strong acids with low pK_a values.

In the structural model proposed to stabilize a higher pK_2 for the CL headgroup, the secondary hydroxyl of the central glycerol plays a critical role as a hydrogen bond donor to the ionized phosphate and as a hydrogen bond acceptor for the phosphate that remains protonated at higher pH [49,50] (Fig. 1B). To test the potential role of this hydroxyl group in our system, we analyzed the pH-dependence of the ζ potential of vesicles containing 20 mol % dCL, which lacks this functional group (Fig. 3C, closed circles, solid line). Based on this analysis, the ionization of the dCL headgroup (pK_2 = 1.64) is similar to that of TOCL, indicating that the central hydroxyl does not significantly impact the dissociation behavior of the CL phosphates. Moreover, it has also been proposed that the lack of an acyl chain on CL may affect ionization properties of the CL headgroup as well [53]. We therefore addressed this in our system by measuring the pH-dependent ζ potential profile of vesicles containing 20 mol% MLCL, a lysolipid form of CL that lacks a single acyl chain (Fig. 3C, open circles, dashed line). Again, we found that the ionization of the MLCL headgroup (pK_2 = 1.36) did not differ significantly from that of TOCL. Therefore, the phosphates of the CL headgroup behave as strong acids with pK_a values that are neither affected by the lack of the central glycerol nor by the lack of an acyl chain.

To provide additional support that the end point of these titrations with CL-containing vesicles represented dianionic species, we performed ζ potential analyses at higher pH values (in the pH range of 8–10) in an AMPD-based buffer (Supplementary Fig. S6). For this analysis, we compared vesicles containing 20 mol% POPS, POPA, and TOCL. POPS, like POPC and POPE is an aminoglycerophospholipid, but is anionic at physiological pH due to the presence of a carboxylic acid group with an intrinsic pK_a of 4.0, and the headgroup of POPA is a primary phosphate with an intrinsic second pK_a of 7.0 [46]. Hence, in the pH range from 8 to 10, we would expect the ψ_0 (and therefore ζ potentials) of these samples to become increasingly negative as the primary amine of POPE became deprotonated. But POPA, with two negative charges, would impart a more negative ζ potential than would POPS, which bears only a single negative charge. Our experimental comparisons of POPS- and POPA-containing vesicles bear out this prediction (Fig. S6A). Comparably, our comparisons of POPS- and TOCL-containing vesicles also show a more negative ζ potential with TOCL, confirming that it is a dianion within this pH range. It should be noted here that due to the lower ionic strength of the AMPD buffer system, the

measured ζ potentials are expected to be more negative than they would be at a given pH in our phosphate/citrate system (Fig. 3) due to reduced electrostatic shielding, lower ion complexation, and greater Debye length (see Supplementary Fig. S4).

Taken together, we conclude based on our electrokinetic analysis that the CL headgroup behaves like a strong dibasic acid in which the pK_a value of each phosphate is low. As a corollary, CL exists as a dianion at physiological pH. Moreover, we conclude that the ionization properties of the phosphates are not influenced by the lack of a central hydroxyl or by the lack of an acyl chain.

3.3. pH-dependent profiles of sizes of vesicles with different lipid composition

We used dynamic light scattering to characterize the size and homogeneity of our liposome samples prepared at different pH values (Fig. 4). The measured diameters (reported here as Z-average values, or harmonic intensity averaged particle diameter) of liposomes containing CL variants were within the expected value for our LUVs across the pH range tested (Fig. 4A). Diameters of PG-containing vesicles were similar, with the exception of those tested at pH 2.0, which indicated larger vesicle sizes. At this pH value close to the *pK*a of PG, we expect that the loss of surface charge – particularly for the monoanoinic PG – could promote vesicle fusion. The measured polydispersity index (Fig. 4B) indicates that the vesicle sizes were reasonably homogeneous at all pH values, again with the exception of PG-containing vesicles at pH 2.0, which were highly heterogeneous. From these results we conclude that within the critical pH range in which we observe complete CL ionization in our zeta potential analyses, our model membranes are stable and there is no appreciable change in their size distributions.

3.4. fluorescence-based analysis of CL ionization within model membranes

As an independent assay for the surface charge of CL-containing model membranes, we used the fluorescent probe 9-AA as a measure of the surface electrostatic potential. At neutral pH, 9-AA has a single positive charge. This cationic probe will therefore accumulate in the diffuse double layer adjacent to negatively charged surfaces and self-quench in a concentration-dependent manner [71]. Hence, 9-AA quenching has been used as a readout of membrane surface electrostatic potential with a variety of lipid systems [67–70]. In the present work, we measured the steady-state fluorescence of 9-AA (λ_{em} = 400 nm, λ_{ex} = 455 nm, see Supplementary Fig. S7A) in the presence of vesicles containing POPG or CL variants while performing time course titrations of cations that lower the magnitude of the surface potential and therefore de-quench the 9-AA signal. For these titrations, we used decamethonium (DM^{2+}), an organic divalent cation that will accumulate in the double layer, thereby screening the surface charge and rendering ψ_0 less negative (Eq. 3), but does not specifically bind to lipid headgroups (K_{DM2+} = 0) and therefore does not affect the σ through ionic complexation (Eq. 5) [70,72]. This latter point simplifies the analysis by obviating potential ambiguities attendant with the specific adsorption of divalent cations to anionic lipids [73]. The underlying premise of this analysis is that among different membranes, equivalent values of 9-AA fluorescence indicate equivalent values of ψ_0, as explained in Supplementary Fig. S5. Here we use POPG-containing vesicles whose σ (and

therefore whose ψ_0) values are known in order to calibrate the readings from CL-containing samples.

Fig. 5A shows a representative 9-AA measurement time course with POPG-containing LUVs. Upon addition of liposomes to a solution containing 20 μM 9-AA, the fluorescence signal is quenched as the probe accumulates in the electric field adjacent to the negatively charged bilayer surface. Progressive addition of DM^{2+} screens the electrostatic potential of the bilayer surfaces, measured as stepwise increases in 9-AA emission, and the final addition of metal cation at high concentration (10 mM $MgCl_2$) effects the complete release of 9-AA quenching, returning the 9-AA signal to the pre-liposome value (F_{max}). We note that under our measurement conditions, the addition of DM^{2+} and $MgCl_2$ has a negligible effect on the intrinsic fluorescence properties of 9-AA (Supplementary Fig. S7B) and that the addition of buffer alone to samples containing 9-AA in the presence of liposomes does not change the signal (Supplementary Fig. S7C), ruling out any significant dilution effects on these readings.

To calibrate the 9-AA readings with respect to surface potential, we performed time course titrations with LUVs containing different molar concentrations of POPG with known charge density at pH 7.5 (σ^{max} = −0.0687, −0.1144, and −0.1602 C m^{-2} for LUVs with 30 mol%, 50 mol%, and 70 mol% POPG, respectively) (Fig. 5B). For each titration point, the associated ψ_0 was calculated based on Gouy–Chapman–Stern formalism (simultaneous evaluation of Eqs. 3–5) and the resulting calibration curve (Fig. 5B, inset) was used to evaluate ψ_0 values of CL-containing samples. Then, identical 9-AA time course measurements were performed for LUVs containing 50 mol% TOCL, dCL and MLCL. Fig. 5C shows representative time traces for these samples in comparison with a sample containing 50 mol% POPG.

The evaluation of surface charge densities of CL-containing vesicles is shown in Fig. 5, panels D–F. For each CL vesicle type, three independent DM^{2+} titrations were performed and the resulting F/F_{max} values were taken as equivalence points to determine surface potential from calibrations curves (as in Supplementary Fig. S5). In each panel from D to F, the calibration curve from panel B is shown (dashed line) in comparison with the mean computed values of ψ_0 (open circles) for each sample set. The consistency of the measured F/F_{max} values is demonstrated by the low variability of the ψ_0 values that fall along the calibration curve. In order to calculate the surface charge densities of each sample based on ψ_0 values, it was necessary to account for adsorption of the 9-AA probe to the bilayer, an issue that has been described by previous investigations using this technique [69,74]. To do this, we included a term for 9-AA binding in our surface charge density equation (Eq. 5) as done previously [74], and used a least-squares fitting analysis with the set of calculated ψ_0 values and simultaneous evaluation of new Eqs. 3–5 to determine the apparent association constants for 9-AA (K_{9AA}^{app}). This returned K_{9AA}^{app} values of 276.2 M^{-1}, 251 M^{-1}, and 203.9 M^{-1} for LUVs containing TOCL, dCL and MLCL, respectively. Values of σ calculated at each titration point accounting for 9-AA binding (panels D–F, closed circles) revealed mean σ values of −0.153 (±0.012) C m^{-2} for TOCL-containing samples, −0.167 (±0.011) C m^{-2} for dCL-containing samples, and −0.168 (±0.012) C m^{-2} for MLCL-containing samples. These values are consistent with CL variants having two electronic charges per headgroup (σ

= −0.153 C m^{-2}, right axes, open arrows) and not with CL variants having a single charge per headgroup (σ = −0.076 C m^{-2}, right axes, closed arrows). Based on this evaluation, we conclude that all CL variants in these samples are fully ionized at pH 7.5.

To be sure, the adsorption of the 9-AA probe to CL-containing samples is a confounding feature of this analysis. However, we note that although 9-AA appears to interact with CL-containing membranes with a nonzero association constant, the interaction is reversible as demonstrated by the complete release of 9-AA quenching upon addition of 10 mM $MgCl_2$ (Fig. 5C). We also note that even if this type of analysis is taken purely as a *relative* comparison of surface charge among model membranes (i.e., without calculation of ψ_0 or σ), it still demonstrates that the 9-AA dequenching profile (Fig. 5C) is identical between samples containing TOCL (for which the intramolecular hydrogen bonding network is theoretically possible) and dCL (which lacks the ability to stabilize disparate pK_a values by intramolecular hydrogen bonding). Identical ionization behavior of TOCL and dCL in the physiological pH range itself can therefore be taken as evidence that the CL headgroup is fully ionized in both cases.

4. Discussion

The central conclusion from this study is that the two phosphates of the cardiolipin headgroup – at physiologically relevant molar concentrations in a lamellar bilayer – each have proton dissociation behavior typical of a strong acid (i.e., with pK_a values near the first pK_a of phosphoric acid). It therefore follows that under such conditions, cardiolipin exists in its fully ionized state (as a dianion) in the physiological pH range. Identical ionization behavior was detected regardless of the presence of the hydroxyl group of the central glycerol (dCL) or the full complement of acyl chains (MLCL).

Surface charge density is central to many properties of biological membranes, and it has particular relevance for CL-containing bilayers. First, the polymorphic phase behavior of CL is strongly dependent on headgroup charge. Like other lipids with conical molecular geometry (a headgroup with a smaller effective cross-sectional area than the hydrocarbon chain region), CL has the propensity to form inverted hexagonal (H_{II}) structures in aqueous solution [15,75]. Yet CL stably forms lamellar phases in isolation, likely due to strong electrostatic repulsion among headgroups [22,23]. The shift toward non-lamellar phases is potentiated by the reduction in CL headgroup charge by protonation, ionic strength, and interactions with cationic metals, basic proteins, and positively charged lipids [16–23]. In turn, the ability of CL to promote negative stress curvature in bilayers is critical for the establishment of highly-curved regions in biomembranes [76], including mitochondrial cristae [77], which can regulate the activation of membrane-associated proteins [78], including tafazzin, the CL transacylase [79]. Second, the headgroup charge is a central factor in the electrostatic attraction and binding of proteins in the interfacial region, including peripheral membrane proteins (e.g., cytochrome c, mitochondrial kinases and apoptotic proteins [80–82]) and integral membrane proteins (e.g., the ADP/ATP carrier and subunits of respiratory complex IV [83, 84]). Moreover, CL is known to specifically coordinate divalent cations with high affinity [14], and the ion:lipid stoichiometry is dependent on the CL headgroup formal charge [73]. Finally, headgroup charge distribution is a determining factor

in the types of nonbonding interactions that can occur among lipids, including electrostatic and hydrogen bonding interactions [85,86]. Clearly, for each of the above phenomena, the ionization state of the CL headgroup is of fundamental importance; whether this lipid exists in the mono- or dianionc state strongly influences its behavior in the bilayer.

Based on pH titration experiments with CL dispersions [49], the dominant view has been that the phosphate groups of CL have strongly disparate ionization behavior (pK_1 ~ 2–4 and pK_2 > 8.5). By contrast, a more recent study also using pH titrations with synthetic CL showed that both phosphates ionize as strong acids with pK_a values ranging between 2.5 and 3.5 [61]. It is noteworthy that in this latter study, support for two low pK_a values also came from calorimetric experiments. Furthermore, the results of a recent FTIR study with CL-containing liposomes were also consistent with the dual ionization of phosphate groups within a range of pH values (4 to 11) [62]. This study obtained clear spectra for small vesicles composed of 100% CL, but vesicles containing only 20% CL could not be interpreted unambiguously. It is, however, noteworthy that previous FTIR studies reported evidence of CL headgroup structure that would in fact promote widely different pK_a values [50,55]. Given that the same experimental approaches have provided some of the strongest empirical support for both of these divergent models of CL ionization, there is a strong need to resolve this issue with alternative techniques, as we have done in this study.

The results of our work support a model in which the headgroup phosphates of CL ionize independently as strong acids. It is important to define exactly what is meant by the pK_a values reported herein. The apparent pK_a value of a titratable group within the context of the bilayer (pK_a^{app}) is the *bulk* pH at which half of the population is ionized. This would be obtained, for instance, by a direct fit of the pH titrations shown in Fig. 3. The intrinsic pK_a (pK_a^{int}), by contrast, can be formally defined as the (here, theoretical) pK_a of the ionizable group that is free in solution. To a first approximation, pK_a^{app} and pK_a^{int} can be related by the electrostatic correction term ($F\psi_0/2.303\ RT$) that accounts for the surface pH (see Supplementary Text, Eq. S2). But as described previously [46,87], proton dissociation behavior of lipid headgroups is modulated by additional “bilayer effects”, including: (i) electrostatic and hydrogen bonding interactions among polar headgroups, and (ii) reduced Born energy of ion hydration in the lower dielectric environment of the interface. Hence, our measured pK_a values for the CL phosphates (~1 to 1.5) are more accurately described as the “surface” pK_a values rather than pK_a^{int}. Apropos of this point, it should be noted that lipid headgroup ionization is dependent upon the lipid environment (e.g., the local concentration of anionic lipids) and protein interactions. The present study used model lipid systems, which do not account for possible pK_a alterations of the CL phosphate groups within protein-rich energy conserving membranes in which this lipid resides. It also does not account for possible localized clustering of CL which, due to electrostatic interactions, could in principle raise the pK_a values of phosphate groups, effectively lowering the surface charge density. CL molecules within such specialized microenvironments of native biomembranes could very well have distinct proton dissociation behavior

The experimental approaches employed herein represent established techniques for the evaluation of lipid bilayer surface charge density. Yet for both approaches, it must be

acknowledged that key assumptions had to be made in the analysis of the data. First, for both the electrokinetic and fluorescence-based approaches, evaluation of the pK_a of the test anionic lipid (CL variants) required input of pK_a values for all other titratable lipid headgroups in the system. Values of lipid headgroup pK_a and association constants for monovalent electrolytes were not measured directly in this study, but rather taken from well-established values in the literature [46,66]. The second point pertains to analysis of electrokinetic data. For the relationship between electrophoretic mobility and the ζ potential (Eq. 1) to be valid, the size of a particle of radius r must be much larger than the Debye length ($1/\kappa$) so that the particle surface can be considered locally planar (i.e., that $\kappa r \gg 1$), a condition met by our samples (Fig. 4). Also critical is the relationship between ζ potential and ψ_0. Within the diffuse double layer of a charged particle surface, the electric potential decays as a function of distance as shown in Supplementary Fig. S3. This means that the magnitude of the ζ potential of the particle measured in an electric field is lower in magnitude than the ψ_0 in a manner depending on the electric potential profile and the location of the hydrodynamic shear plane. In our analyses, the plane of shear was assumed to be 2 Å from the surface, as substantiated previously [66]. Moreover, we assume that the dielectric constant and viscosity of the aqueous phase (Eqs. 1 and 3) are independent of the distance from the surface. We note, however, that these assumptions were applied equally to all samples and that although they impact the calculation of the *absolute* ψ_0, they do not affect *relative* comparisons between samples (e.g., PG- and CL-containing samples) or the *shapes* of the titration curves, which were used to determine pK_a values (Fig. 3). We note also that ζ potential measurements have been widely used to measure surface charge and ionization properties of acidic lipids in vesicles, and that the results are in excellent agreement with other techniques [66,88,89]. The final point pertains to our fluorescence-based analysis. As noted, this approach is predicated on the assumption that 9-AA emission intensity is a readout of surface potential such that equivalence of probe fluorescence between two samples indicates equal ψ_0 [67,69,70,74]. This approach provides a direct comparison between liposomes of identical lipid composition; however, as described previously, one must also account for specific binding of the probe to anionic lipids, particularly CL [69,74]. By evaluating complete datasets of 9-AA titrations that included probe binding, we obtained apparent 9-AA association constants that yield values of σ in excellent agreement with a prediction of complete CL ionization (Fig. 5). However, we stress again that even if these 9-AA profiles are taken simply as relative indicators of surface charge without mathematical analyses, they still show identical correspondence between vesicles with TOCL and dCL (Fig. 5C). If, as suggested, the central hydroxyl is required for stabilizing the two disparate pK_a values [49,50], we would expect significantly different profiles between the TOCL- and dCL-containing samples, which we do not observe. On these grounds alone, therefore, these results indicate complete ionization of the CL headgroup at physiological pH.

Finally, the results of this study have relevance for the role of CL biogenesis in human disease. Barth syndrome is caused by mutations in the gene encoding tafazzin, the mitochondria-located transacylase involved in the CL remodeling pathway. Owing to defects in the MLCL reacylation step of CL remodeling, Barth syndrome patients display abnormal CL acyl chain profiles, decreased overall CL mass, and a buildup of MLCL [38–42]. Using

yeast as a model eukaryote, a recent study used a panel of knockouts in the CL remodeling pathway to show that unremodeled CL, resulting form knockouts in the Cld1p deacylase, appeared to support mitochondrial functions as well as remodeled CL [90]. This suggests that the underlying cause of Barth syndrome may not be altered acyl chain composition per se, but rather an increase in MLCL/CL ratio. This possibility was supported by an earlier study with a *Drosophila* model of Barth syndrome and Barth syndrome patient lymphoblasts, which showed that genetic or pharmacological inactivation of the iPLA2 phospholipase suppressed the phenotype of tafazzin deficiency [33]. Along the same lines, it was previously proposed that MLCL may exert a deleterious effect by altering the anchorage of the lipid in the bilayer, and subsequently disrupting headgroup intramolecular hydrogen bonding and ionization properties [53]. However, by demonstrating that MLCL has headgroup ionization properties identical to tetraacyl CL, the present study shows that the effects of increased MLCL in mitochondrial membranes is not due to alteration of its proton dissociation behavior or formal charge. Instead, the effect of MLCL is more likely related to its altered molecular geometry and/or altered interactions with lipids and proteins within the hydrocarbon core.

Supplementary Material

Refer to Web version on PubMed Central for supplementary material.

Acknowledgments

We would like to thank the members of the Alder Research Group for stimulating discussions during the preparation of this work. This work was supported by National Institutes of Health Grant 1R01GM113092, National Science Foundation Grant MCB-1330695, and Barth Syndrome Foundation Research Grant (to N.N.A.).

Abbreviations

AMPD	2-amino-2-methyl-1,3-propanediol
POPC	1-palmitoyl-2-oleoyl-*sn*-glycero-3-phosphocholine
POPE	1-palmitoyl-2-oleoyl-*sn*-glycero-3-phosphoethanolamine
POPG	1-palmitoyl-2-oleoyl-*sn*-glycero-3-phosphoglycerol
POPA	1-palmitoyl-2-oleoyl-*sn*-glycero-3-phosphate
POPS	1-palmitoyl-2-oleoyl-*sn*-glycero-3-phosphoserine
TOCL	1′,3′-bis[1,2-dioleoyl-*sn*-glycerol-3-phospho-]-*sn*-glycerol
dCL	2′-deoxycardiolipin
MLCL	monolyso-cardiolipin

References

1. Arias-Cartin R, Grimaldi S, Arnoux P, Guigliarelli B, Magalon A. Cardiolipin binding in bacterial respiratory complexes: structural and functional implications. Biochim Biophys Acta. 2012; 1817:1937–1949. [PubMed: 22561115]
2. Chaban Y, Boekema EJ, Dudkina NV. Structures of mitochondrial oxidative phosphorylation supercomplexes and mechanisms for their stabilisation. Biochim Biophys Acta. 2014; 1837:418–426. [PubMed: 24183696]
3. Mileykovskaya E, Dowhan W. Cardiolipin-dependent formation of mitochondrial respiratory supercomplexes. Chem Phys Lipids. 2014; 179:42–48. [PubMed: 24220496]
4. Paradies G, Paradies V, De Benedictis V, Ruggiero FM, Petrosillo G. Functional role of cardiolipin in mitochondrial bioenergetics. Biochim Biophys Acta. 2014; 1837:408–417. [PubMed: 24183692]
5. Claypool SM, Koehler CM. The complexity of cardiolipin in health and disease. Trends Biochem Sci. 2012; 37:32–41. [PubMed: 22014644]
6. Joshi AS, Zhou J, Gohil VM, Chen S, Greenberg ML. Cellular functions of cardiolipin in yeast. Biochim Biophys Acta. 2009; 1793:212–218. [PubMed: 18725250]
7. Li XX, Tsoi B, Li YF, Kurihara H, He RR. Cardiolipin and its different properties in mitophagy and apoptosis. J Histochem Cytochem. 2015; 63:301–311. [PubMed: 25673287]
8. Mileykovskaya E, Dowhan W. Cardiolipin membrane domains in prokaryotes and eukaryotes. Biochim Biophys Acta. 2009; 1788:2084–2091. [PubMed: 19371718]
9. Planas-Iglesias J, Dwarakanath H, Mohammadyani D, Yanamala N, Kagan VE, Klein-Seetharaman J. Cardiolipin interactions with proteins. Biophys J. 2015
10. Shi Y. Emerging roles of cardiolipin remodeling in mitochondrial dysfunction associated with diabetes, obesity, and cardiovascular diseases. J Biol Res. 2010; 24:6–15.
11. Shen Z, Ye C, McCain K, Greenberg ML. The role of cardiolipin in cardiovascular health. Biomed Res Int. 2015; 2015:891707. [PubMed: 26301254]
12. Jefferies JL. Barth syndrome. Am J Med Genet C: Semin Med Genet. 2013; 163C:198–205. [PubMed: 23843353]
13. Gaspard GJ, McMaster CR. Cardiolipin metabolism and its causal role in the etiology of the inherited cardiomyopathy Barth syndrome. Chem Phys Lipids. 2015; 193:1–10. [PubMed: 26415690]
14. Lewis RN, McElhaney RN. The physicochemical properties of cardiolipin bilayers and cardiolipin-containing lipid membranes. Biochim Biophys Acta. 2009; 1788:2069–2079. [PubMed: 19328771]
15. van den Brink-van der Laan E, Killian JA, de Kruijff B. Nonbilayer lipids affect peripheral and integral membrane proteins via changes in the lateral pressure profile. Biochim Biophys Acta. 2004; 1666:275–288. [PubMed: 15519321]
16. Seddon JM, Kaye RD, Marsh D. Induciton of the lamellar-inverted hexagonal phase transition in cardiolipin by protons and monovalent cations. Biochim Biophys Acta. 1983; 734:347–352.
17. Dahlberg M. Polymorphic phase behavior of cardiolipin derivatives studied by coarse-grained molecular dynamics. J Phys Chem B. 2007; 111:7194–7200. [PubMed: 17542632]
18. Sankaram MB, Powell GL, Marsh D. Effect of acyl chain composition on salt-induced lamellar to inverted hexagonal phase transitions in cardiolipin. Biochim Biophys Acta. 1989; 980:389–392. [PubMed: 2713413]
19. Vail WJ, Stollery JG. Phase changes of cardiolipin vesicles mediated by divalent cations. Biochim Biophys Acta. 1979; 551:74–84. [PubMed: 106890]
20. Vasilenko I, De Kruijff B, Verkleij AJ. Polymorphic phase behaviour of cardiolipin from bovine heart and from *Bacillus subtilis* as detected by 31P-NMR and freeze-fracture techniques. Effects of Ca^{2+}, Mg^{2+}, Ba^{2+} and temperature. Biochim Biophys Acta. 1982; 684:282–286. [PubMed: 6799000]
21. Trusova VM, Gorbenko GP, Molotkovsky JG, Kinnunen PK. Cytochrome c-lipid interactions: new insights from resonance energy transfer. Biophys J. 2010; 99:1754–1763. [PubMed: 20858419]

22. Lewis RN, McElhaney RN. Surface charge markedly attenuates the nonlamellar phase-forming propensities of lipid bilayer membranes: calorimetric and (31)P-nuclear magnetic resonance studies of mixtures of cationic, anionic, and zwitterionic lipids. Biophys J. 2000; 79:1455–1464. [PubMed: 10969007]
23. Tarahovsky YS, Arsenault AL, MacDonald RC, McIntosh TJ, Epand RM. Electrostatic control of phospholipid polymorphism. Biophys J. 2000; 79:3193–3200. [PubMed: 11106623]
24. Allegrini PR, Pluschke G, Seelig J. Cardiolipin conformaiton and dynamics in bilayer membranes as seen by deuterium magnetic resonance. Biochemistry. 1984; 23:6452–6458.
25. Schlame M, Ren M, Xu Y, Greenberg ML, Haller I. Molecular symmetry in mitochondrial cardiolipins. Chem Phys Lipids. 2005; 138:38–49. [PubMed: 16226238]
26. Schlame M. Cardiolipin remodeling and the function of tafazzin. Biochim Biophys Acta. 2013; 1831:582–588. [PubMed: 23200781]
27. Baile MG, Lu YW, Claypool SM. The topology and regulation of cardiolipin biosynthesis and remodeling in yeast. Chem Phys Lipids. 2014; 179:25–31. [PubMed: 24184646]
28. Ye C, Shen Z, Greenberg ML. Cardiolipin remodeling: a regulatory hub for modulating cardiolipin metabolism and function. J Bioenerg Biomembr. 2014
29. Schlame M. Cardiolipin synthesis for the assembly of bacterial and mitochondrial membranes. J Lipid Res. 2008; 49:1607–1620. [PubMed: 18077827]
30. Ren M, Phoon CK, Schlame M. Metabolism and function of mitochondrial cardiolipin. Prog Lipid Res. 2014; 55:1–16. [PubMed: 24769127]
31. Beranek A, Rechberger G, Knauer H, Wolinski H, Kohlwein SD, Leber R. Identification of a cardiolipin-specific phospholipase encoded by the gene CLD1 (YGR110W) in yeast. J Biol Chem. 2009; 284:11572–11578. [PubMed: 19244244]
32. Xu Y, Malhotra A, Ren M, Schlame M. The enzymatic function of tafazzin. J Biol Chem. 2006; 281:39217–39224. [PubMed: 17082194]
33. Malhotra A, Edelman-Novemsky I, Xu Y, Plesken H, Ma J, Schlame M, Ren M. Role of calcium-independent phospholipase A2 in the pathogenesis of Barth syndrome. Proc Natl Acad Sci U S A. 2009; 106:2337–2341. [PubMed: 19164547]
34. Li J, Romestaing C, Han X, Li Y, Hao X, Wu Y, Sun C, Liu X, Jefferson LS, Xiong J, Lanoue KF, Chang Z, Lynch CJ, Wang H, Shi Y. Cardiolipin remodeling by ALCAT1 links oxidative stress and mitochondrial dysfunction to obesity. Cell Metab. 2010; 12:154–165. [PubMed: 20674860]
35. Cao J, Liu Y, Lockwood J, Burn P, Shi Y. A novel cardiolipin-remodeling pathway revealed by a gene encoding an endoplasmic reticulum-associated acyl-CoA: lysocardiolipin acyltransferase (ALCAT1) in mouse. J Biol Chem. 2004; 279:31727–31734. [PubMed: 15152008]
36. Taylor WA, Hatch GM. Identification of the human mitochondrial linoleoylcoenzyme A monolysocardiolipin acyltransferase (MLCL AT-1). J Biol Chem. 2009; 284:30360–30371. [PubMed: 19737925]
37. Clarke SL, Bowron A, Gonzalez IL, Groves SJ, Newbury-Ecob R, Clayton N, Martin RP, Tsai-Goodman B, Garratt V, Ashworth M, Bowen VM, McCurdy KR, Damin MK, Spencer CT, Toth MJ, Kelley RI, Steward CG. Barth syndrome. Orphanet J Rare Dis. 2013; 8:23. [PubMed: 23398819]
38. Schlame M, Kelley RI, Feigenbaum A, Towbin JA, Heerdt PM, Schieble T, Wanders RJ, DiMauro S, Blanck TJ. Phospholipid abnormalities in children with Barth syndrome. J Am Coll Cardiol. 2003; 42:1994–1999. [PubMed: 14662265]
39. Xu Y, Condell M, Plesken H, Edelman-Novemsky I, Ma J, Ren M, Schlame M. A *Drosophila* model of Barth syndrome. Proc Natl Acad Sci U S A. 2006; 103:11584–11588. [PubMed: 16855048]
40. Vreken P, Valianpour F, Nijtmans LG, Grivell LA, Plecko B, Wanders RJ, Barth PG. Defective remodeling of cardiolipin and phosphatidylglycerol in Barth syndrome. Biochem Biophys Res Commun. 2000; 279:378–382. [PubMed: 11118295]
41. Gu Z, Valianpour F, Chen S, Vaz FM, Hakkaart GA, Wanders RJ, Greenberg ML. Aberrant cardiolipin metabolism in the yeast taz1 mutant: a model for Barth syndrome. Mol Microbiol. 2004; 51:149–158. [PubMed: 14651618]

42. McKenzie M, Lazarou M, Thorburn DR, Ryan MT. Mitochondrial respiratory chain supercomplexes are destabilized in Barth syndrome patients. J Mol Biol. 2006; 361:462–469. [PubMed: 16857210]
43. Gennis, RB. Biomembranes Molecular Structure and Function. Springer-Verlag; New York: 1989.
44. Horvath SE, Daum G. Lipids of mitochondria. Prog Lipid Res. 2013; 52:590–614. [PubMed: 24007978]
45. Marsh, D. Handbook of Lipid Bilayers. 2. CRC Press; Boca Raton: 2013.
46. Tocanne JF, Teissie J. Ionization of phospholipids and phospholipid-supported interfacial lateral diffusion of protons in membrane model systems. Biochim Biophys Acta. 1990; 1031:111–142. [PubMed: 2155023]
47. Few AV, Gilby AR, Seaman GV. An electrophoretic study on structural components of micrococcus lysodeikticus. Biochim Biophys Acta. 1960; 38:130–136. [PubMed: 13822582]
48. Coulon-Morelec MJ, Faure M, Marechal J. Controlled degradation of diphosphatidylglycerol (cardiolipid) in an acid medium. Study of the phosphatide derivatives obtained. Bull Soc Chim Biol (Paris). 1962; 44:171–183. [PubMed: 13881708]
49. Kates M, Syz JY, Gosser D, Haines TH. pH-dissociation characteristics of cardiolipin and its 2′-deoxy analogue. Lipids. 1993; 28:877–882. [PubMed: 8246687]
50. Hubner W, Mantsch HH, Kates M. Intramolecular hydrogen bonding in cardiolipin. Biochim Biophys Acta. 1991; 1066:166–174. [PubMed: 1854782]
51. Haines TH. Anionic lipid headgroups as a proton-conducting pathway along the surface of membranes: a hypothesis. Proc Natl Acad Sci U S A. 1983; 80:160–164. [PubMed: 6296863]
52. Haines TH, Dencher NA. Cardiolipin: a proton trap for oxidative phosphorylation. FEBS Lett. 2002; 528:35–39. [PubMed: 12297275]
53. Haines TH. A new look at cardiolipin. Biochim Biophys Acta. 2009; 1788:1997–2002. [PubMed: 19801076]
54. Nichols-Smith S, Kuhl T. Electrostatic interactions between model mitochondrial membranes. Colloids Surf B: Biointerfaces. 2005; 41:121–127. [PubMed: 15737537]
55. Hielscher R, Wenz T, Hunte C, Hellwig P. Monitoring the redox and protonation dependent contributions of cardiolipin in electrochemically induced FTIR difference spectra of the cytochrome bc(1) complex from yeast. Biochim Biophys Acta. 2009; 1787:617–625. [PubMed: 19413949]
56. Sidiq S, Verma I, Pal SK. pH-driven ordering transitions in liquid crystal induced by conformational changes of cardiolipin. Langmuir. 2015; 31:4741–4751. [PubMed: 25856793]
57. Aguayo D, Gonzalez-Nilo FD, Chipot C. Insight into the properties of cardiolipin containing bilayers from molecular dynamics simulations, using a hybrid all-atom/united-atom force field. J Chem Theory Comput. 2012; 8:1765–1773. [PubMed: 26593668]
58. Dahlberg M, Marini A, Mennucci B, Maliniak A. Quantum chemical modeling of the cardiolipin headgroup. J Phys Chem A. 2010; 114:4375–4387. [PubMed: 20187622]
59. Lemmin T, Bovigny C, Lancon D, Dal Peraro M. Cardiolipin models for molecular simulations of bacterial and mitochondrial membranes. J Chem Theory Comput. 2013; 9:670–678. [PubMed: 26589063]
60. Pan J, Cheng X, Sharp M, Ho CS, Khadka N, Katsaras J. Structural and mechanical properties of cardiolipin lipid bilayers determined using neutron spin echo, small angle neutron and X-ray scattering, and molecular dynamics simulations. Soft Matter. 2015; 11:130–138. [PubMed: 25369786]
61. Olofsson G, Sparr E. Ionization constants pKa of cardiolipin. PLoS ONE. 2013; 8:e73040. [PubMed: 24058458]
62. Malyshka D, Pandiscia LA, Schweitzer-Stenner R. Cardiolipin containing liposomes are fully ionized at physiological pH. An FT-IR study of phosphate group ionization. Vib Spectrosc. 2014; 75:86–92.
63. Aveyard, R.; Haydon, DA. An Introduction to the Principles of Surface Chemistry. Cambridge University Press; London: 1973.
64. Ohshima, H. Biophysical Chemistry of Interfaces. Wiley; Hoboken: 2010.

65. McLaughlin S. Electrostatic potentials at membrane–solution interfaces. Curr Top Membr Transp. 1977; 9:71–144.

66. Eisenberg M, Gresalfi T, Riccio T, McLaughlin S. Adsorption of monovalent cations to bilayer membranes containing negative phospholipids. Biochemistry. 1979; 18:5213–5223. [PubMed: 115493]

67. Barber J. Membrane surface charges and potentials in relation to photosynthesis. Biochim Biophys Acta. 1980; 594:253–308. [PubMed: 7018576]

68. Berczi A, Moller IM. Surface charge density estimation by 9-aminoacridine fluorescence titration: improvements and limitations. Eur Biophys J. 1993; 22:177–183.

69. Brauer DK, Yermiyahu U, Rytwo G, Kinraide TB. Characteristics of the quenching of 9-aminoacridine fluorescence by liposomes made from plant lipids. J Membr Biol. 2000; 178:43–48. [PubMed: 11058686]

70. Chow WS, Barber J. Salt-dependent changes of 9-aminoacridine fluorescence as a measure of charge densities of membrane surfaces. J Biochem Biophys Methods. 1980; 3:173–185. [PubMed: 7451810]

71. Searle GF, Barber J. The involvement of the electrical double layer in the quenching of 9-aminoacridine fluorescence by negatively charged surfaces. Biochim Biophys Acta. 1978; 502:309–320. [PubMed: 26393]

72. Fiolet JW, Bakker EP, van Dam K. The fluorescent properties of acridines in the presence of chloroplasts or liposomes. On the quantitative relationship between the fluorescence quenching and the transmembrane proton gradient. Biochim Biophys Acta. 1974; 368:432–445. [PubMed: 4451661]

73. Cohen JA, Cohen M. Adsorption of monovalent and divalent cations by phospholipid membranes. The monomer–dimer problem. Biophys J. 1981; 36:623–651. [PubMed: 7326327]

74. Kicq P, Meutter JD, Goormaghtigh E, Caspers J, Ruysschaert JM. Use of 9-aminoacridine in the evaluation of liposome surface charge density: role of the adsorption of lipidic sites. Bioelectrochem Bioenerget. 1987; 17:277–285.

75. de Kruijff B. Lipid polymorphism and biomembrane function. Curr Opin Chem Biol. 1997; 1:564–569. [PubMed: 9667894]

76. Renner LD, Weibel DB. Cardiolipin microdomains localize to negatively curved regions of *Escherichia coli* membranes. Proc Natl Acad Sci U S A. 2011; 108:6264–6269. [PubMed: 21444798]

77. Schlame M, Ren M. The role of cardiolipin in the structural organization of mitochondrial membranes. Biochim Biophys Acta. 2009; 1788:2080–2083. [PubMed: 19413994]

78. Epand RM, D'Souza K, Berno B, Schlame M. Membrane curvature modulation of protein activity determined by NMR. Biochim Biophys Acta. 2015; 1848:220–228. [PubMed: 24835017]

79. Schlame M, Acehan D, Berno B, Xu Y, Valvo S, Ren M, Stokes DL, Epand RM. The physical state of lipid substrates provides transacylation specificity for tafazzin. Nat Chem Biol. 2012; 8:862–869. [PubMed: 22941046]

80. Kagan VE, Tyurin VA, Jiang J, Tyurina YY, Ritov VB, Amoscato AA, Osipov AN, Belikova NA, Kapralov AA, Kini V, Vlasova Q II, Zhao M, Zou P, Di DA, Svistunenko IV, Kurnikov GG. Borisenko, Cytochrome c acts as a cardiolipin oxygenase required for release of proapoptotic factors. Nat Chem Biol. 2005; 1:223–232. [PubMed: 16408039]

81. Shamas-Din A, Bindner S, Chi X, Leber B, Andrews DW, Fradin C. Distinct lipid effects on tBid and Bim activation of membrane permeabilization by pro-apoptotic Bax. Biochem J. 2015; 467:495–505. [PubMed: 25714678]

82. Schlattner U, Tokarska-Schlattner M, Ramirez S, Bruckner A, Kay L, Polge C, Epand RF, Lee RM, Lacombe ML, Epand RM. Mitochondrial kinases and their molecular interaction with cardiolipin. Biochim Biophys Acta. 2009; 1788:2032–2047. [PubMed: 19409873]

83. Nury H, Dahout-Gonzalez C, Trezeguet V, Lauquin G, Brandolin G, Pebay-Peyroula E. Structural basis for lipid-mediated interactions between mitochondrial ADP/ATP carrier monomers. FEBS Lett. 2005; 579:6031–6036. [PubMed: 16226253]

84. Arnarez C, Marrink SJ, Periole X. Identification of cardiolipin binding sites on cytochrome c oxidase at the entrance of proton channels. Sci Rep. 2013; 3:1263. [PubMed: 23405277]

85. Pinheiro TJ, Duralski AA, Watts A. Phospholipid headgroup–headgroup electrostatic interactions in mixed bilayers of cardiolipin with phosphatidylcholines studied by 2H NMR. Biochemistry. 1994; 33:4896–4902. [PubMed: 8161549]

86. Boggs JM. Lipid intermolecular hydrogen bonding: influence on structural organization and membrane function. Biochim Biophys Acta. 1987; 906:353–404. [PubMed: 3307919]

87. Egorova EM. Dissociation constants of lipid ionizable groups I. Corrected values for two anionic lipids, colloids and surfaces A. Physiochem Eng Aspects. 1998; 131:7–18.

88. Matos C, de Castro B, Gameiro P, Lima JL, Reis S. Zeta-potential measurements as a tool to quantify the effect of charged drugs on the surface potential of egg phosphatidylcholine liposomes. Langmuir. 2004; 20:369–377. [PubMed: 15743080]

89. McLaughlin S, Harary H. The hydrophobic adsorption of charged molecules to bi-layer membranes: a test of the applicability of the stern equation. Biochemistry. 1976; 15:1941–1948. [PubMed: 946770]

90. Baile MG, Sathappa M, Lu YW, Pryce E, Whited K, McCaffery JM, Han X, Alder NN, Claypool SM. Unremodeled and remodeled cardiolipin are functionally indistinguishable in yeast. J Biol Chem. 2014; 289:1768–1778. [PubMed: 24285538]

Appendix A. Supplementary data

Supplementary data to this article can be found online at http://dx.doi.org/10.1016/j.bbamem.2016.03.007.

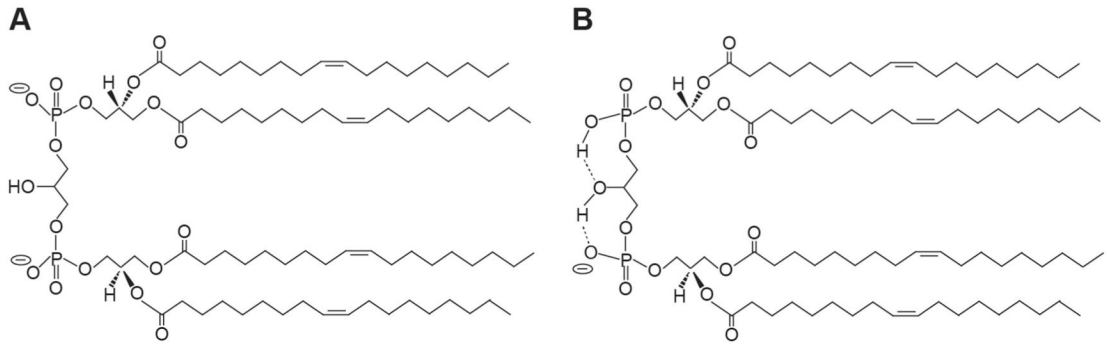

Fig. 1.

Cardiolipin structure. Chemical structures of tetraoleoyl cardiolipin (1′,3′-bis[1,2-dioleoyl-*sn*-glycero-3-phospho]-*sn*-glycerol) representing the two models of headgroup ionization state at physiological pH. A) Low *pK*a values of both phosphates. In this model, both phosphates ionize independently, each assuming proton dissociation behavior corresponding to the first protolysis step of phosphoric acid. Thus the headgroup exists as a dianion at physiological pH. B) Disparate *pK*a values of the two phosphates. In this model, the phosphates form a bicyclic ring structure above the two *sn*-1 acyl chains, which is stabilized by resonance (not shown). In this acid-anion structure, the secondary hydroxyl of the central glycerol mediates hydrogen bonding interactions (dashed lines) that stabilize the protonated form of one phosphate and the headgroup exists as a monoanion at physiological pH.

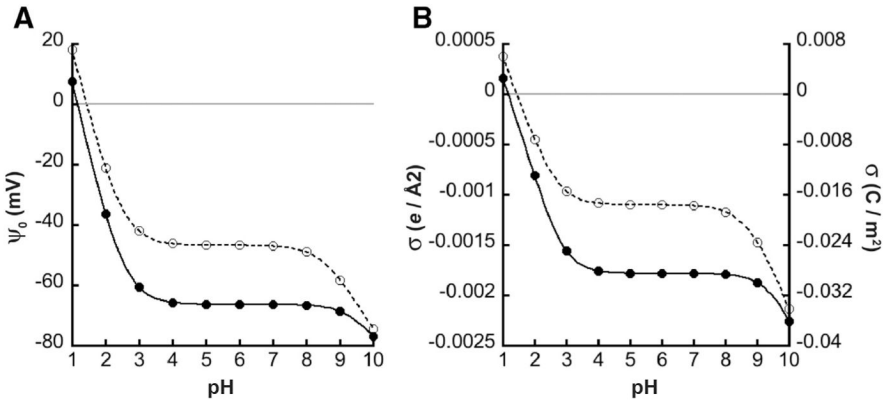

Fig. 2.

Electrostatic properties of bilayers differing in CL ionization behavior. Using Gouy–Chapman–Stern formalism (simultaneous evaluation of Eqs. 3–5), the bulk pH-dependent profiles of A) surface potential (ψ_0) and B) surface charge density (σ) were calculated for a ternary lipid bilayer consisting of 20 mol% CL in a background of PC and PE ($\chi_{PC} = 0.4$, $\chi_{PE} = 0.4$, $\chi_{CL} = 0.2$). The model included a bulk concentration of 20 mM symmetrical monovalent electrolyte (C^+A^-) wherein counterions specifically bound charged lipid headgroup species with an association constant $K_M = 1.0\ M^{-1}$. Intrinsic pK_a values for PC and PE functional groups are described in Supplementary Fig. S1. Case 1 (closed symbols, solid lines): the intrinsic pK_a values of the two phosphates of CL are identical ($pK_1 = 1.0$; $pK_2 = 1.0$). Case 2 (open symbols, dotted lines): disparate intrinsic pK_a values of the two phosphate groups of CL ($pK_1 = 1.0$; $pK_2 = 8.5$).

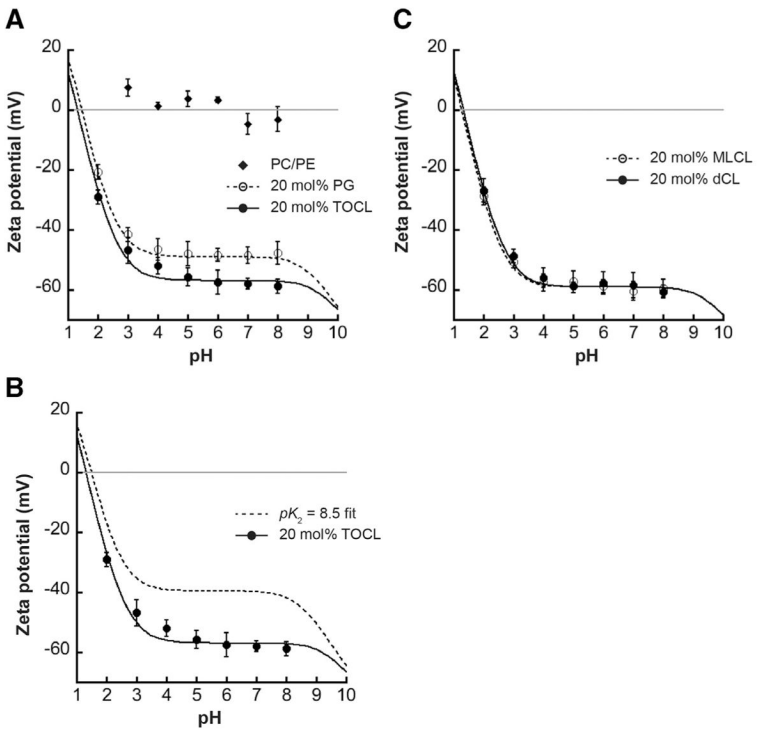

Fig. 3.

pH-dependent ζ potential profiles. Measurements of ζ potential for LUVs of defined lipid composition in a phosphate/citrate buffer system are shown for each value of bulk pH (symbols are mean values of a minimum of three independent samples; error bars are SD). Lines indicate fits to the data based on Gouy–Chapman–Stern analysis. pK_a values reported below are based on acid dissociation constants of phosphate groups from data fits; for CL-containing samples, it is assumed that $pK_1 = 1.0$. A) Composite ζ potential profile for vesicles containing POPC/POPE host lipids only (diamonds), 20 mol% POPG (open circles, dashed line; $pK_a = 0.99$) or 20 mol% TOCL (closed circles, solid line; $pK_2 = 1.59$). B) Measured ζ potential profile for TOCL-containing vesicles (closed circles, dashed line, $pK_1 = 1.0$ and $pK_2 = 1.59$) shown with the calculated profile of the same lipid system wherein TOCL phosphates have disparate ionization constants (dashed line, $pK_1 = 1.0$ and $pK_2 = 8.5$). C) Measured ζ potential profiles for vesicles containing 20 mol% MLCL (open circles, dashed line; $pK_2 = 1.36$) and 20 mol% dCL (closed circles, solid line; $pK_2 = 1.64$).

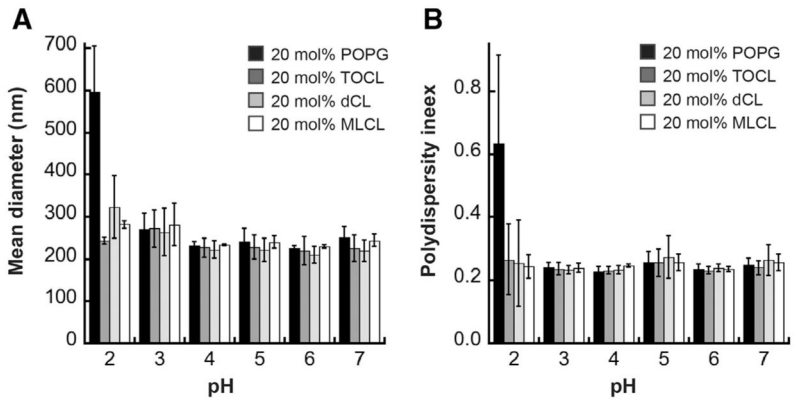

Fig. 4.

pH-dependent liposome size distribution. A) Average diameters (reported as Z-average values) and B) polydispersity indeces of liposomes prepared in a POPE/POPE background with 20 mol% POPG (black) TOCL (dark gray), dCL (light gray) or MLCL (white) at the indicated pH values, as measured by dynamic light scattering. Each value represents an average of three independent measurements; error bars are standard deviations.

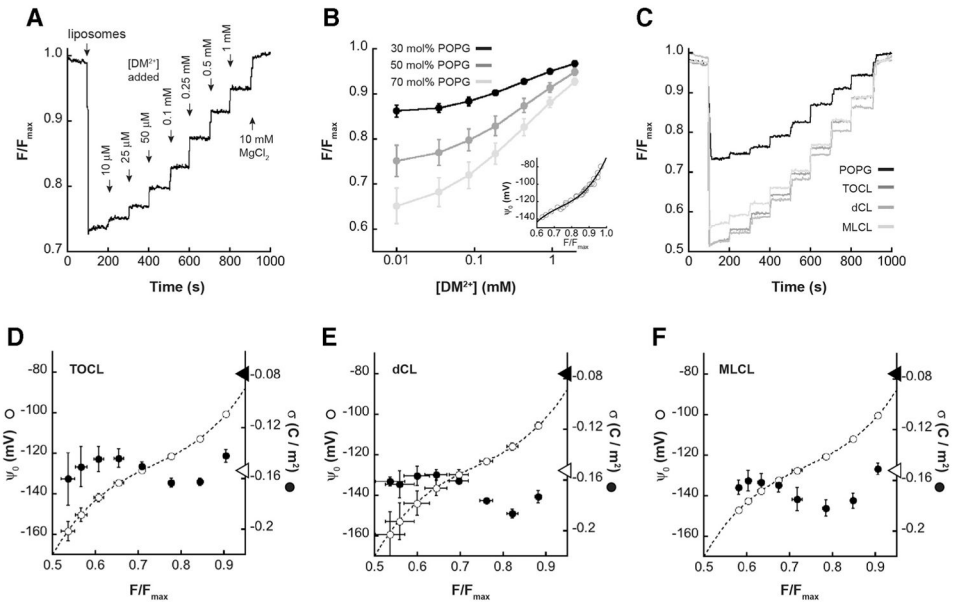

Fig. 5.

9-AA analysis of surface charge density. LUVs with different concentrations of anionic phospholipid were subjected to time course titrations with DM^{2+} in the presence of the fluorescent probe 9-AA. Steady-state measurements of 9-AA fluorescence were normalized to the maximal value following $MgCl_2$ addition and quantified as F/F_{max}. A) Representative time course of 9-AA fluorescence with LUVs containing 50 mol% POPG, showing addition of liposomes, titration of DM^{2+}, and final addition of $MgCl_2$. B) Measured values of F/F_{max} (means with SD, n = 3 independent measurements) as a function of [DM^{2+}] for LUVs with varying concentrations of POPG as indicated. *Inset*, calibration curve relating ψ_0 and F/F_{max} based on 9-AA data with POPG-containing LUVs. The ψ_0 values were calculated based on the relevant σ^{max} values (−0.0687, −0.1144, and −0.1602 C m^{-2} for LUVs with 30, 50 and 70 mol% POPG, respectively). C) Time courses of 9-AA fluorescence with LUVs containing 50 mol% CL variants (TOCL, dCL or MLCL in dark, medium and light gray as indicated) in comparison with LUVs containing 50 mol% POPG (black). D–F) Profiles of ψ_0 and σ for LUVs containing the indicated CL variants based on 9-AA steady-state readings (means with SD, n = 3 independent measurements). Dashed lines show the fit to the ψ_0 vs. F/F_{max} calibration curve (panel B, inset). Open circles show the calculated ψ_0 based on the eight different equivalence point measurements (see Supplementary Fig. S5). Closed circles show calculated σ based on 9-AA K_M^{app} values (276.2 M^{-1}, 251.5 M^{-1}, and 203.9 M^{-1} for TOCL, dCL and MLCL, respectively). Arrowheads on the surface potential axis represent σ values corresponding to one electronic charge per CL headgroup (closed arrowhead) and two electronic charges per CL headgroup (open arrowhead).